Hindawi
Advances in Materials Science and Engineering
Volume 2022, Article ID 7692772, 11 pages
https://doi.org/10.1155/2022/7692772

Research Article

Monitoring and Analysis of a High-Performance Concrete Shaft Lining: A Case Study

Daolu Quan,[1,2] Hongguang Ji,[1,2] Xiaobo Su,[1,2] Hui Cao,[1] and Juanhong Liu[1,2]

[1]*College of Civil and Resource Engineering, University of Science and Technology Beijing, Beijing 100083, China*
[2]*Key Laboratory of Urban Underground Space Engineering, University of Science and Technology Beijing, Beijing 100083, China*

Correspondence should be addressed to Hongguang Ji; 1274242908@qq.com

Received 13 December 2021; Revised 5 January 2022; Accepted 8 January 2022; Published 31 January 2022

Academic Editor: Ren Fuqiang

Shaft lining in ultradeep mines on the coast of eastern China under the complex external environments of "high in situ stress and high osmotic pressure" has the disadvantages of failure; to solve this problem, the field test of high-performance concrete shaft lining structure was carried out in Sha-ling gold mine. The field test study of the high-performance concrete shaft lining was carried out in a −1120 m ingate and a −1114 m to −1124 m shaft. Its stress and deformation were monitored and analyzed. The maximum compressive stress of the HPC shaft lining structure at the level of −1117.7 m of the air intake shaft is 1.91 MPa. Based on the Von-Mises yield theory and the analytical solution of thick-walled cylinder theory, the ultimate limit of the high-performance concrete shaft lining in the Sha-ling gold mine was obtained. The high-performance concrete shaft lining strain changes smoothly, and concrete strain can be divided into three stages: the rapid growth period, the slow growth period, and the stable period. The monitoring results show that the high-performance concrete shaft lining has excellent mechanical properties in the external environment of high in situ stress, which can be used as a reference for the support design of similar projects.

1. Introduction

Under the complex external environments of "high in situ stress, high ground temperature, high water pressure, and strong excavation disturbance" [1], the physical and mechanical properties of deep rock masses are generally different from those of shallow rock masses [2, 3]; thus, the rock masses change from an elastic state to a plastic state. The pressure distribution of the surrounding rock and the excavation disturbance stress path will affect the stability of the surrounding rock. To study the fatigue failure characteristics of sandstone, Zhu et al. carried out cyclic loading and unloading numerical simulation tests of sandstone with different loading parameters and different water content [4]. Gao et al. studied the mechanical properties of coal at various mining rates on the laboratory scale and the field scale [5]. Chen et al. adopted an analytical approach to calculate the equivalent elastic modulus of fractured rock masses with a random discrete fracture or regular fracture considering the confining stress [6]. In the process of shaft excavation, water inrush, rock-burst, lamping, and other engineering support problems are frequent occurrences. Some high-grade shaft lining concrete may even suffer brittle failure in the deep external environment of high in situ stress and high osmotic pressure. Simultaneously, the deep strata and deep-water quality in the coastal area are rich in Cl^- and SO_4^{2-} ions, putting the shaft lining concrete at risk of chemical corrosion [7–9], which seriously affects the strength and durability of the concrete [10–13] and dramatically shortens the life of the shaft lining.

Stress-strain monitoring technology has been widely used in geotechnical and underground engineering. Zhu et al. monitored and analyzed the deformation of deep foundation pit, ground subsidence, and adjacent buildings [14]. Dou et al. studied the influence of shear displacement on fluid flow and solute transport in three-dimensional rough fractures of fractured rock mass [15]. Cao et al. used the interferometric synthetic aperture radar (InSAR) technology to obtain the ground surface deformation [16]. Dou et al. investigated the influence of the layer transition

zone on the multilayered slope [17]. The shaft lining structures' stress, deformation, and strength characteristics have been studied using model tests [18–24]. Ding et al. analyzed the failure characteristics and mechanical mechanism of the slope by the physical model test [25]. Zhao et al. analyzed the plastic limit load of shaft lining based on the unified strength theory and discussed the relationship between the plastic limit load of shaft lining and the strength difference of structural materials [26]. Lyu and Wang monitored and analyzed the shaft lining deformation of the weakly cemented stratum in west China and obtained the limit deformation value of the shaft lining [27]. To study the mechanical behavior of surrounding rock under prestressed bolt support, Li et al. established the mechanical model of bolt support, and the deformation of the surrounding rock of the inclined shaft was monitored [28]. However, previous studies on the shaft lining support form usually focus on the topsoil layer; however, few reports focus on the shaft lining stress and deformation characteristics under the occurrence of the complex external environments of "high in situ stress and high osmotic pressure" in the deep stratum.

As for the deep shaft support method of metal mine, there is no mature theory so far. In the environment of high in situ stress in the deep stratum, drilling in rock mass or supporting by high-grade concrete is usually adopted to resist the large deformation of surrounding rock. However, Liu et al. presented that high-grade concrete (C50 and above) has an impact tendency and brittle failure will occur [29]. It is of engineering significance to study and use the high-performance concrete shaft lining with low impact tendency to control the deformation of surrounding rock under the environment of high in situ stress of deep metal mine.

Hence, based on the −1114 m to −1124 m section of the air intake shaft and the −1120 m ingate high-performance concrete (HPC) shaft lining structure field application research in this paper, we analyze the characteristics of stress and deformation of high-performance concrete shaft lining. Combined with the Von-Mises yield theory and thick-walled cylinder theory, the ultimate stress of the high-performance concrete shaft lining is established. The strain variation law of the HPC shaft lining is obtained. The advantages and disadvantages of the applications of HPC are summarized. It is hopeful that our work can provide a reference for a deep metal shaft lining structure design.

2. Engineering Geological

2.1. Engineering Background. As shown in Figure 1, the Sha-ling gold mine is located in Lai-Zhou City, Shandong Province. The linear distance between the northwest end of the mining area and the coast of the Bohai Sea is about 5.3 km, which belongs to the coastal area of Shandong Province. The distance between the main shaft, the auxiliary shaft, and the air intake shaft in the Sha-ling gold mine is relatively close, which is approximately triangular in space, and the linear distance between the auxiliary shaft and the air intake shaft is about 60 m.

The design depth of the air intake shaft within the Sha-ling gold mine is 1449 m, the net diameter of the shaft lining is 6.5 m, and the thickness of the support is 400 mm, which was excavated using a common method. The original support design parameters of the shaft from −1114 m to −1124 m and the ingate at −1120 m of air intake shaft are exhibited in Table 1.

2.2. Geological Background. The regional geological structure of the Sha-ling gold mine construction project is complex, and the fault structure is developed within the area. The main fault is the Jiao-Jia fault, the branch fault is the Wang-Er-Shan fault, and the north section fault is the Ling-Shan fault. The rock fissures are developed on both sides of the Jiao-Jia fault zone. The upper part of the Jiao-Jia fault is metamorphic gabbro and the lower part of the Jiao-Jia fault is dominated by granite. The rock mass from −1114 m to −1124 m is sericeous granite, and the quality grade of rock mass is grade II. The uniaxial compressive strength of sericite granite in this section is about 90 MPa. RQD value approaches 48%, and the rock mass is comparatively broken.

3. Distribution of In Situ Stress in Sha-Ling Gold Mine

Understanding the law of in situ distribution is the basis for investigating deep rock mechanics [30] in order to obtain the in situ stress distribution law of the deep strata in the shaft construction area of the Sha-ling gold mine and guide the shaft excavation. Before the shaft excavation, our research group used the hydraulic fracturing method to measure the in situ stress in the Sha-ling gold mine. In the in situ measurement of the air intake shaft in the Sha-ling gold mine, the drill pipe cannot be lowered because of the serious hole collapse. The linear distance between the auxiliary shaft and the air intake shaft is about 60 m, so the in situ measurement is carried out in the auxiliary shaft. The hydraulic fracturing in situ stress measurement equipment adopted the SY- 2007 single-loop in situ stress measurement system developed by the Institute of Geomechanics, Chinese Academy of Geological Sciences [31]. The law of in situ stress distribution in the auxiliary shaft of the Sha-ling gold mine is shown in Figure 2.

It can be seen from Figure 2 that the maximum horizontal principal stress in the shaft construction engineering area is 24.14 MPa~45.56 MPa (−775.4 m~−1532.5 m), and the minimum horizontal principal stress is 18.85 MPa~37.51 MPa (−775.4 m~−1532.5 m). The maximum and minimum horizontal principal stress near −1120 m is 35.9 MPa and 27.2 MPa, respectively.

4. Field Test Method

4.1. Raw Materials and Mixture Proportions. The HPC of the deep shaft is composed of silicate 42.5R cement, a special compound comprised of river sand, copper-plated microwire steel fiber, and a polycarboxylic acid water reducer. The mixtures' proportions of the HPC in the deep shaft are

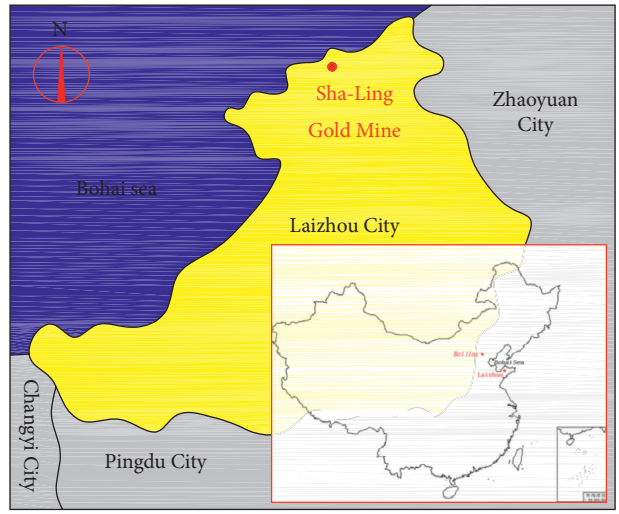

Figure 1: Location of Sha-ling gold mine.

Table 1: The original support parameters of −1114 m to −1124 m shaft lining and the −1120 m ingate of the air intake shaft.

Deep	Support parameter	
	Primary support	Second-time support
−1120 m ingate	Bolt type: MSGLW-335/20 × 2000; bolt density: 1 m × 1 m; butterfly tray: 150 × 150 × 10; density of steel mesh: 120 × 120 Rebar diameter: 6 mm	C30 reinforced concrete, support thickness: 400 mm; outer reinforced: HΦ22@250VΦ18@250 Inner reinforced: HΦ22@250VΦ18@250; stirrup: Φ10@500 ∗ 500
−1114 m to −1124 m	No	Ditto

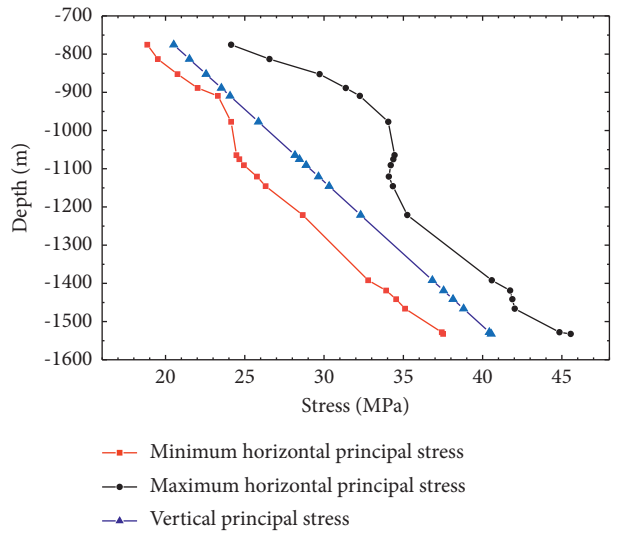

Figure 2: In situ stress distribution of auxiliary shaft in Sha-ling gold mine.

present in Table 2. The compound is composed of finely ground slag powder, fly ash, and silica fume proportions. Its performance meets the requirements of the concrete cementing materials and the compressive strength of the HPC reaches 80 MPa. Zhou et al. studied the splitting tensile strength, flexural strength, brittleness coefficient, impact energy index, dynamic failure time, and other parameters of the HPC through rigorous laboratory tests [32]. The brittleness coefficient, impact energy index, dynamic failure time, and other parameters of the HPC belong to the category of nonimpact liability, which will not be elaborated in detail in this paper.

In order to complete the field test research on the −1120 m ingate of the air intake shaft (the ingate support is

Table 2: Mixing proportions of HPC.

Composition	Cement ($kg \cdot m^{-3}$)	Special admixtures ($kg \cdot m^{-3}$)	Sand ($kg \cdot m^{-3}$)	Steel fiber ($kg \cdot m^{-3}$)	Water ($kg \cdot m^{-3}$)	Admixture ($kg \cdot m^{-3}$)	Water-binder ratio
Proportion	240	630	1205	50	200	10	0.23

5 m) and the −1114 m to −1124 m HPC shaft lining, approximately 120 m^3 of HPC was prepared on-site. The HPC was mixed evenly with a mixer and transported to the casting layer using a bucket. When the concrete was mixed, steel fiber was added in batches in order to evenly disperse the material and ensure the workability of the concrete. The HPC after mixing is shown in Figure 3, and the HPC shaft lining after the mold removal is shown in Figure 4.

4.2. Field Monitoring Instruments

4.2.1. Force-Measuring Bolt. The environment of the deep shaft in coastal areas is harsh. The complex external environments, such as high ground temperature and water drenching from the large shaft lining, put forth higher requirements for monitoring the instruments' reliability and durability. To cope with the complex external environments of the deep shaft and ensure the authenticity and reliability of the monitoring results, an improved stress monitoring sensor force-measuring bolt was used to monitor shaft lining stress. As shown in Figure 5, the force-measuring bolt is composed of three parts: the steel bar meter, the steel bar, and a steel plate within the PVC pipe. The steel bar meter is connected to both ends of the steel bar; one end of the steel bar is welded to a steel plate. The steel plate length × width is 150 × 150 mm, and the thickness is 6 mm. The force measurement bolt is 900 mm long.

Before the concrete shaft lining is poured, one end of the unconnected steel plate is fixed to the surrounding rock. The steel bar placed deep into the surrounding rock is then fixed into the surrounding rock via epoxy resin. Both ends of the PVC pipe are sealed to avoid the reinforcement meter being interfered with by the vibrations caused by the pouring of concrete into the shaft lining; thus reducing the probability of the reinforcement meter being corroded by groundwater. This instrument has been used, and its reliability has been proven in the stress monitoring of the new main shaft at -1300 m and -1418 m levels within the Xin-Cheng gold mine [33].

4.2.2. Vibrating String Concrete Strain Gauge. The concrete strain monitoring sensor uses an embedded vibrating string concrete strain gauge. The standard measuring range of the embedded vibrating string concrete strain gauge is ±3000 $\mu\varepsilon$, and the working environment temperature is −25~80°C, confirmed with a temperature measuring function.

When the strain gauge is buried in concrete, the vibration frequency of the vibrating string in the strain gauge changes with the deformation of the concrete. The strain size of the strain gauge can be obtained by using the vibration frequency change of the vibrating string; thus, the strain change of the concrete can be measured. The strain calculation formula of the vibrating string strain gauge can be expressed as

$$\varepsilon = k\left(f_i^2 - f_0^2\right) + T_K\left(T_i - T_0\right), \quad (1)$$

where ε is the strain relative to the initial time, $\mu\varepsilon$; k is the conversion coefficient, $k = 2.48 \times 10^{-3}$; f_i is the output frequency, $\mu\varepsilon$; f_0 is the original frequency, $\mu\varepsilon$; T_K is the coefficient for temperature correction, $T_K = 2.2$; T_i is the temperature value at the time of measurement, °C; T_0 is tne initial temperature, °C.

4.3. Test Point Arrangement. Figure 6 illustrates the layout of the stress and strain monitoring points on the shaft lining from −1114 m to −1124 m of the air intake shaft and the ingate from −1120 m. Three measuring points were arranged at the arch and the left and right shoulders of the ingate at 1120 m. Three measuring points were arranged on the shaft lining connected with the ingate. The three measuring points on the shaft lining were all at the same level with the waistline of the ingate (−1117.7 m). One load bolt, one circumferential concrete strain gauge, and one axial concrete strain gauge were installed at each measuring point. Data collection was carried out after concrete pouring, and 3~4 groups of data were collected at each measuring point for a total of 30 days.

5. Results and Analysis

5.1. Stress Characteristics and Analysis of the HPC Shaft Lining at −1117.7 m Level. The shaft lining stress variation of the HPC at the −1117.7 m level is shown in Figure 7. The tensile stress of the shaft lining is positive, and the compressive stress is negative. It can be seen from Figure 7 that the interaction stresses between the high-performance concrete shaft lining and the surrounding rock are compressive stress at measurement points No. 1, 2, and 3 at −1117.7 m level. The shaft lining restricts the movement of the surrounding rock to the surface of the wellbore so that the interaction stress between the shaft lining and the surrounding rock is compressive. The stress of the surrounding rock is adjusted continuously, and the interaction stress between the shaft lining and surrounding rock is in a fluctuating state. During the monitoring period, the interaction stress at measuring point No. 1 is 0.029~0.056 MPa, the interaction stress at measuring point No. 2 is 0.016~0.038 MPa, and the interaction stress at measuring point No. 3 is 0.33~1.91 MPa.

The interaction stress between shaft lining and surrounding rock at −1117.7 m level of measuring point No. 3 increases slowly at first. After 18 days of high-performance concrete pouring, the interaction stress between shaft lining and surrounding rock at measuring point No. 3 increases rapidly and finally stabilizes at 1.8 MPa. The compressive

Figure 3: HPC after mixing.

Figure 4: HPC shaft lining after form stripping.

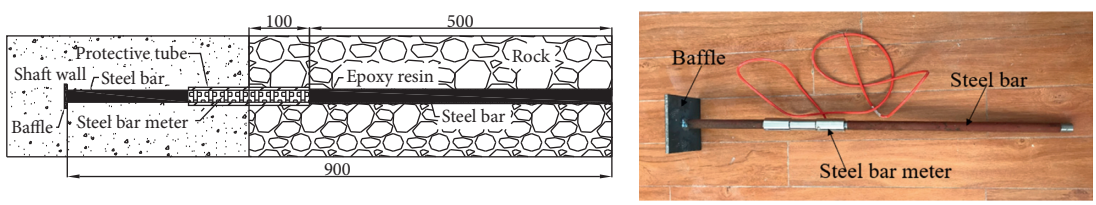

(a) (b)

Figure 5: The force-measuring anchor. (a) Monitoring diagram of the force-measuring anchor. (b) Image of the force-measuring anchor.

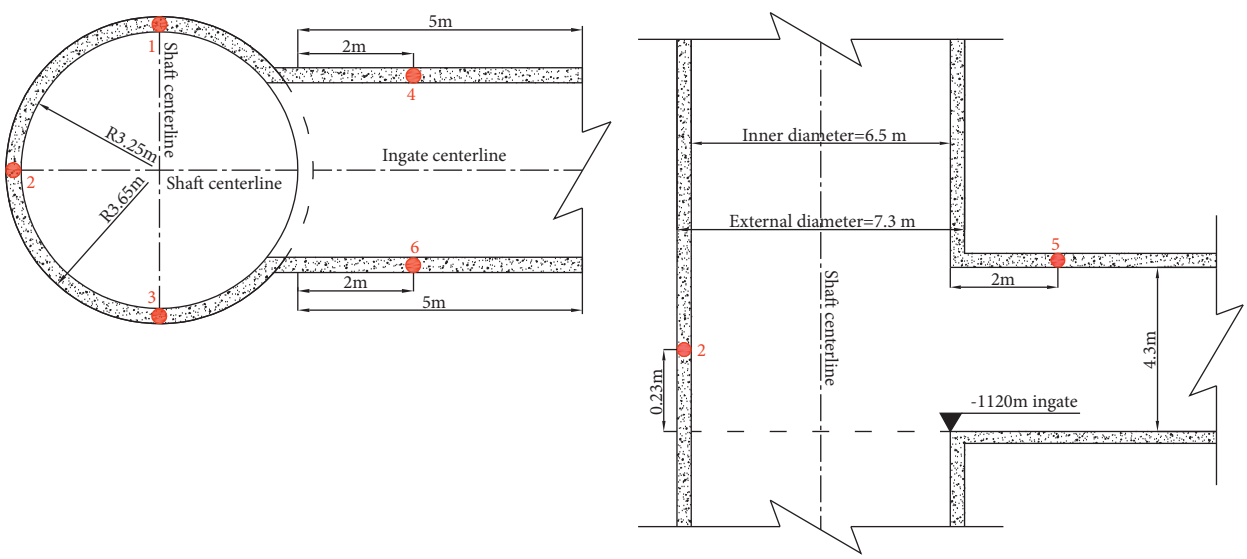

(a) (b)

Figure 6: Layout of measuring points.

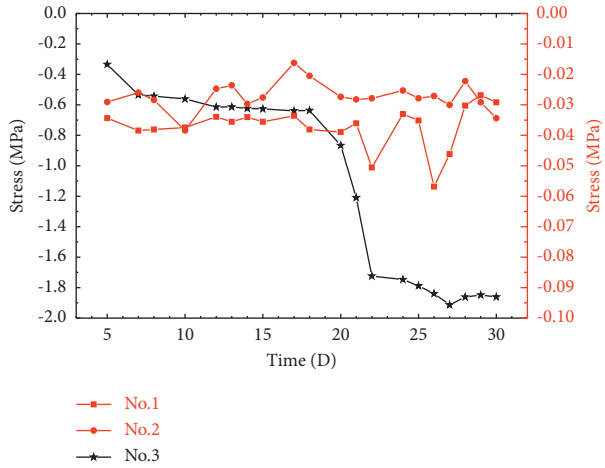

Figure 7: Variations of interaction stress between the horizontal shaft lining and the surrounding rock at the −1117.7 m shaft lining.

stresses between shaft lining and surrounding rock at measuring points No. 1 and 2 are small, and the maximum value is only 0.055 MPa. As can be seen from Figure 8, the circumferential strains of concrete at measuring points No. 1 and 2 are finally maintained at 500 $\mu\varepsilon$ and 600 $\mu\varepsilon$, respectively, which indicates that the surrounding rock at No. 1 and No. 2 has large deformation under the action of high in situ stress. Thus, the interaction stresses between shaft lining and surrounding rock at measuring points No. 1 and 2 should be larger because the surrounding rock produces higher circumferential stress to the shaft lining. However, the value of interaction stresses between shaft lining and surrounding rock at measuring points No. 1 and 2 is small, and the change law of interaction stress is not consistent with the strain evolution of concrete. The analysis shows that the hole diameter is too large when the force-measuring anchors were buried at measuring points No. 1 and 2. The lack of occlusion between the steel bar of the force anchor and the surrounding rock leads to the nonsynchronous movement which results in a small interaction stress between the surrounding rock and the shaft lining+.

5.1.1. Ultimate Stress of the High-Performance Concrete Shaft Lining at −1117.7 m Level. The calculation diagram of stress distribution of surrounding rock during circular shaft excavation is shown in Figure 9.

When $r = r_0$, the stress distribution of surrounding rock can be expressed as

$$\begin{aligned} \sigma_{rr} &= 0, \\ \sigma_{r\theta} &= P[(1+\lambda) - 2(1-\lambda)\cos 2\theta], \\ \tau_{r\theta} &= 0, \end{aligned} \tag{2}$$

where σ_{rr} is the rock radial stress, $\sigma_{r\theta}$ is the rock tangential stress, $\tau_{r\theta}$ is the rock shearing stress, P is the initial stress, and λ is the nonuniform coefficient.

Yu et al. according to the calculation diagram of stress distribution of surrounding rock during circular shaft excavation provided, the criterion for judging whether surrounding rock enters a plastic state is introduced [34]:

$$\sigma_{r\theta} = P[(1+\lambda) - 2(1-\lambda)\cos 2\theta] \geq R_c, \tag{3}$$

where R_c is the uniaxial compressive strength of rock.

According to equation (3), if the tangential stress of the surrounding rock is higher than the compressive strength of the rock, the surrounding rock enters the plastic state. Otherwise, the surrounding rock is in an elastic state. The measured maximum horizontal principal stress and minimum principal stress of Sha-ling gold mine at −1120 m are 35.9 MPa and 27.2 MPa, respectively, and the compressive strength of surrounding rock is about 90 MPa. Thus, the surrounding rock is in an elastic state after the vertical shaft −1120 m is excavated in the Sha-ling gold mine.

At present, there is no reasonable formula for determining the bearing capacity of the high-performance concrete shaft lining. The Von-Mises yield theory is adopted in the design code of the mine chamber in China. Therefore, based on the Von-Mises yield theory and thick-walled cylinder theory, the formula for calculating the ultimate bearing capacity of the high-performance concrete shaft lining is obtained. The Von-Mises strength criteria are as follows:

$$\sqrt{(\sigma_1 - \sigma_2)^2 + (\sigma_1 - \sigma_3)^2 + (\sigma_2 - \sigma_3)^2} \leq \sqrt{2} f_c, \tag{4}$$

where σ_1 is the first principal stress, σ_2 is the second principal stress, σ_3 is the third principal stress, and f_c is the axial compressive strength of concrete prism, MPa.

Assuming that the shaft lining is the homogeneous and continuous isotropic material, the stress solution of the shaft lining under the action of lateral pressure can be known from the stress law of the thick-walled cylinder [35]:

$$\begin{aligned} \sigma_{sr} &= -\frac{b^2 p_0}{b^2 - a^2}\left(1 - \frac{a^2}{r^2}\right), \\ \sigma_{s\theta} &= -\frac{b^2 p_0}{b^2 - a^2}\left(1 + \frac{a^2}{r^2}\right), \\ \sigma_{sz} &= \nu(\sigma_r + \sigma_\theta). \end{aligned} \tag{5}$$

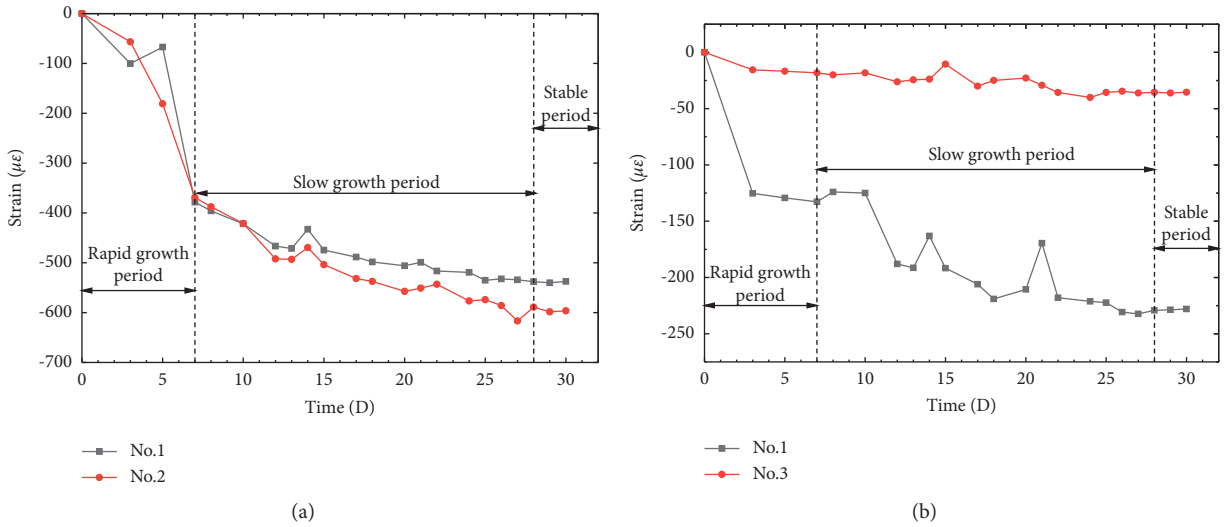

Figure 8: Strain variation of HPC at a depth of −1117.7 m. (a) Circumferential strain of HPC. (b) Axial strain of HPC.

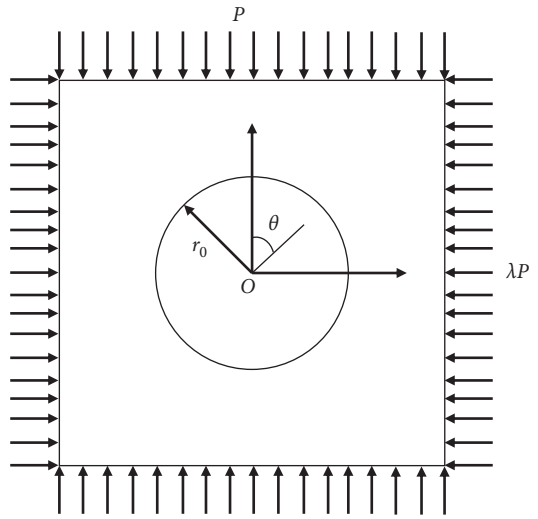

Figure 9: Stress calculation model of surrounding rock of circular shaft.

where a is the radius of inner shaft lining, b is the radius of external shaft lining, p_0 is the uniform external pressure on the shaft lining, σ_{sr} is the normal stress of shaft lining, $\sigma_{s\theta}$ is the circumferential stress shaft lining, σ_{sz} is the vertical stress shaft lining, ν is Poisson's ratio of concrete, and $\sigma_{sr} > \sigma_{sz} > \sigma_{s\theta}$.

Substituting equation (5) into the Von-Mises strength criterion equation (4), the stress of the concrete shaft lining can be decomposed as follows:

$$p_0 = \frac{f_c\left(b^2 - a^2\right)}{b^2\sqrt{3a^4/r^4 + 4\nu^2 - 4\nu + 1}}. \tag{6}$$

Neglecting the stress concentration of high-performance concrete, the shaft lining enters a plastic state at $r = a$. Therefore, the ultimate stress of the concrete shaft lining can be expressed as

$$p_0 = \frac{f_c\left(b^2 - a^2\right)}{b^2\sqrt{4\nu^2 - 4\nu + 4}}. \tag{7}$$

Poisson's ratio of high-performance concrete is 0.14~0.23 [36]. Poisson's ratio of high-performance concrete in this study is 0.2, and its uniaxial compressive strength is about 80 MPa. The radius of the inner shaft lining is $a = 3.25$ m, the radius of the external shaft lining is$b = 3.65$ m. Taking the above parameters into equation (7), the ultimate stress of the HPC shaft lining in the Sha-ling gold mine is 9.04 MPa.

During the monitoring period, the maximum stress at the measuring point No. 3 of the shaft lining at −1117.7 m level is 1.91 MPa. Obviously, the compressive stress of high-performance concrete shaft lining will not reach its limit stress, and the high-performance concrete shaft lining can

meet the support needs of metal mines in the complex environment of high in situ stress.

5.2. Stress Characteristics and Analysis of the HPC Shaft Lining at −1120 m Ingate. The interaction stresses between shaft lining and surrounding rock of the three measuring points at a depth of −1120 m of the ingate vault as well as the left and right arch shoulders are shown in Figure 10. The interaction stresses between the shaft lining and the surrounding rock at the three measuring points are tension stress which indicates that the shaft lining and the surrounding rock at the three measuring points of the ingate show the trend of tension or shear movement. The interaction stress between the shaft lining and surrounding rock of measuring point No. 4 is 0.61~1.73 MPa, the stress of measuring point No. 5 is 1.03~2.06 MPa, and the stress of measuring point No. 6 is 1.41~2.4 MPa.

The interaction stresses between the surrounding rock and the shaft lining of the three measuring points of the ingate's high-performance concrete shaft lining are tension. The analysis shows that it may be related to the distribution of stress fields in the Sha-ling gold mine. The maximum horizontal principal stress at −1120 m in the Sha-ling gold mine is 34.09 MPa, and the vertical principal stress is 29.65 MPa, which is 1.15 times that of the vertical principal stress. The maximum principal stress direction is near the NW direction. Influenced by the distribution of the in situ stress field in the Sha-ling gold mine construction area, the three measuring points of the ingate vault and the left and right shoulders were all subjected to tensile stress. The opening of the ingate air intake shaft within the Sha-ling gold mine is due south, and the angle with the direction of the maximum principal stress is approximately 45°. The vertical principal stresses at the arch and left and right shoulders of the ingate are less than the maximum horizontal principal stress. Therefore, the surrounding rock stress of the ingate under the maximum horizontal principal stress is higher than the surrounding rock stress under the vertical principal stress. With the excavation of the shaft, the surrounding rock at the vault and shoulder of the ingate is broken. With the stress adjustment, the surrounding rock at the vault and shoulder slips to both sides, and the acting stress of the surrounding rock on the shaft lining is mainly shear stress, causing the interaction stress between the shaft lining and the surrounding rock to be the pulling stress.

5.3. Strain Variation and Analysis of the HPC Shaft Lining at −1117.7 m Level. Figures 8(a) and 8(b) are the strain variation of the HPC shaft lining at −1117.7 m level. The axial concrete strain gauge at measuring point No. 2 and the circumferential concrete strain gauge at measuring point No. 3 are damaged, and no data was collected. Overall, the concrete strains at the three measuring points of the HPC shaft lining show a trend of first increasing and then stabilizing. The strain change can be divided into three periods: the rapid growth period, the slow growth period, and the stable period.

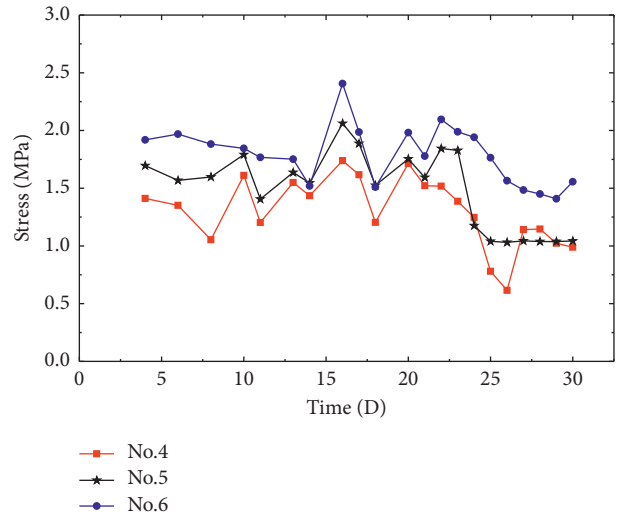

Figure 10: Variations of the interaction stress between the horizontal shaft lining and the surrounding rock at an ingate depth of −1120 m.

In the first seven days after HPC pouring, the circumferential strain at measuring point No. 1 reaches −378 $\mu\varepsilon$, which is 70% of the maximum strain during the monitoring period, and the circumferential strain at point No. 2 reaches −369 $\mu\varepsilon$, which is 60% of the maximum strain during the monitoring period. The axial strain of measuring point No. 1 reaches 132 $\mu\varepsilon$, which is 56% of its maximum strain during the monitoring period. The axial strain of measuring point No. 3 is −18 $\mu\varepsilon$, which is 45% of its maximum strain during the monitoring period. In the first seven days after high-performance concrete pouring, the strain growth rates of the three measuring points are more than 45%, and the strain of high-performance concrete is in the stage of a rapid period. After the casting of the HPC, under the constraint of the surrounding rock, the cementing material is hydrated. As the strength of concrete increases, the constraints of the surrounding rock increase leading to the fact that the strain of the concrete increases rapidly.

From the 8th day to the 28th day after high-performance concrete pouring, the strain growth rate of high-performance concrete decreases obviously. The circumferential strain of measuring point No. 1 increases from −378 $\mu\varepsilon$ to −537 $\mu\varepsilon$, increasing by 159 $\mu\varepsilon$; the circumferential strain of measuring point No. 2 increases from −369 $\mu\varepsilon$ to −588 $\mu\varepsilon$, increasing by 219 $\mu\varepsilon$; the axial strain of measuring point No. 1 increases from −132 $\mu\varepsilon$ to −229 $\mu\varepsilon$, increasing by 97 $\mu\varepsilon$; and the axial strain of measuring point No. 3 increases from −18 $\mu\varepsilon$ to −35 $\mu\varepsilon$, increasing by 17 $\mu\varepsilon$. From the 8th day to the 28th day after HPC pouring, the strain growth rate of HPC slows down obviously. The analysis shows that the hydration of high-performance concrete is basically completed in the first 7 days after pouring, the stiffness and strength of concrete are improved, and the deformation pressure of surrounding rock on shaft lining decreases which leads to the fact that the increasing trend of concrete strain slows down.

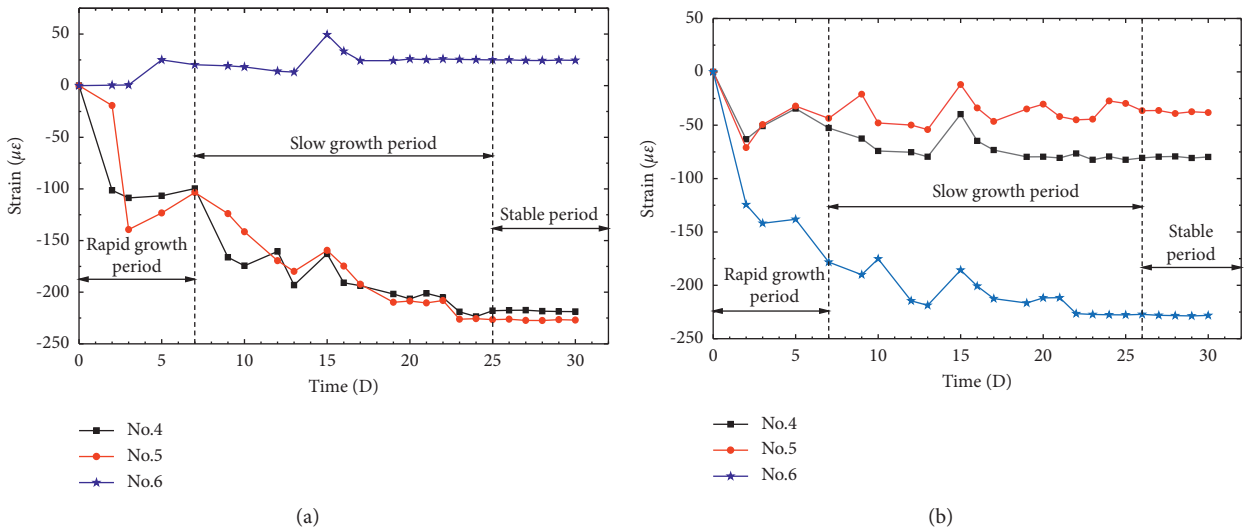

Figure 11: Strain variation of HPC for −1120 m ingate. (a) Circumferential strain of HPC for ingate. (b) Axial strain of HPC for ingate.

5.4. Strain Variation and Analysis of the HPC Shaft Lining at −1120 m Level. Figures 11(a) and 11(b) show the changes of the circumferential and axial strain of HPC at an ingate depth of −1120 m. As seen from Figure 11, the circumferential strains of HPC at measuring points No. 4 and No. 5 of the ingate are compressive, while the circumferential strain of the concrete at measuring point 6 is tensile. The axial strains of the HPC measuring points No. 4, 5, and 6 are all compressive strains. The strain variation law at −1120 m the HPC of the ingate is consistent with that of the −1117.7 m HPC shaft lining: the concrete strain increases rapidly from the completion of casting to the 7th day after the casting. The concrete strain increases slowly from the 8th day to the 28th day after the casting. After 28 days, the concrete strain is stable, and the strain does not change. Compared with the strain change of the shaft linings concrete at −1117.7 m, the strain growth rate at a depth of −1120 m ingate in the first 7 days is lower.

6. Discussion on the Application of the High-Performance Concrete Shaft Lining

The low impact liability of HPC is reflected in the uniform stress of the HPC shaft lining structure and the stable strain change of the HPC. Under the influence of high in situ stress and strong excavation disturbance, the stress of the HPC shaft lining is uniform, which reduces the stress concentration effect and cuts off the path of sudden energy release at a certain point in the concrete under the action of a concentrated stress. The strain change of the HPC shaft lining is stable, and there are no sharp strain increases or continuous fluctuations, indicating that the ability to accumulate elastic strain energy in HPC is poor.

The low impact liability of HPC shaft linings is related to three factors: (1) there are no coarse aggregates in the HPC, the concrete has good fluidity, and the scale of the internal fabric interface decreases, increasing the compactness of the concrete. (2) Steel fibers have a toughening effect on concrete. When steel fiber is added to the HPC, the concrete's ultimate stress and strain will increase. Simultaneously, the steel fibers are interwoven and bonded within the shaft lining, which effectively prevents the expansion of the cracks and slows down the development of microcracks in the concrete [37]. The friction effect of the interface between the fiber, the concrete, and the tension effect of the fiber itself weakens the deformation energy storage of the concrete. (3) The mixture of high-performance concrete contains fly ash and mineral powder. The addition of fly ash and mineral powder enhances the ability of concrete to resist creep and the strain change of concrete is stable.

High-performance concrete has the advantages of high strength, good durability, and small deformation. However, high-performance concrete also has the disadvantages of easy to appear surface cracks in the construction process and high cost compared with ordinary concrete. At the same time, with the increase of external temperature, the porosity and pore diameter of HPC continues to increase, the internal mesostructure deteriorates, and the compressive strength decreases [38]. The high ground temperature environment in deep strata also limits the wide application of the high-performance concrete shaft lining.

7. Conclusions

In this study, the in situ stress of the Sha-ling gold mine is measured and analyzed, the field application test of high-performance concrete shaft lining is carried out, and the strain variation law of high-performance concrete shaft lining is analyzed. Combined with the distribution of in situ stress and the change law of surrounding rock, the stress change characteristics of the shaft lining are analyzed. The conclusions are drawn:

(1) The maximum compressive stress of the HPC shaft lining structure at the level of −1117.7 m of the air intake shaft in the Sha-ling gold mine is 1.91 MPa, and the compressive stress of the high-performance

concrete shaft lining will not reach its limit stress. The HPC shaft lining can meet the complex supporting of the metal mine depth shaft in a coastal area.

(2) The maximum tensile stress of the HPC shaft lining at a depth of −1120 m of the ingate vault as well as the left and right arch shoulders is 2.4 MPa, which is influenced by the in situ stress distribution in the Sha-ling gold mine. The surrounding rock of −1120 m ingate is separated from the shaft lining which results in tensile stress in the ingate vault as well as the left and right arch shoulders.

(3) According to the measured strain data of the high-performance concrete shaft lining at −1117.7 m level and −1120 m ingate in Sha-ling gold mine, it can be seen that the strain change can be divided into three stages: the rapid growth period, the slow growth period, and the stable period. The circumferential strain growth rate of the HPC shaft lining is higher than the axial strain growth rate.

Data Availability

The monitoring data (Excel and origin) used to support the findings of this study are included within the article.

Conflicts of Interest

The authors declare that they have no conflicts of interest.

Acknowledgments

This work was supported by the State Key Research Development Program of China (Grant no. 2016YFC0600801) and Fundamental Research Funds for the Central Universities (06500229); The authors thank AiMi Academic Services (https://www.aimieditor.com) for English language editing and review services.

References

[1] M. C. He, H. P. Xie, P. Peng, and Y.-D. Jiang, "Study on rock mechanics in deep mining engineering," *Chinese Journal of Rock Mechanics and Engineering*, vol. 24, no. 16, pp. 2803–2813, 2005.

[2] L. Zhang, S. Z. Wang, and L. Q. Shi, "Strength characteristics of six kinds of rocks in China under high confining pressure," *Chinese Journal of Rock Mechanics and Engineering*, vol. 4, no. 1, pp. 10–19, 1985.

[3] H. W. Zhou, H. P. Xie, and J. P. Zuo, "Research progress of rock mechanical behavior under deep high ground stress," *Advance in Mechanics*, vol. 35, no. 1, pp. 91–99, 2005.

[4] C. Zhu, M.-c. He, B. Jiang, X.-z. Qin, Q. Yin, and Y. Zhou, "Numerical investigation on the fatigue failure characteristics of water-bearing sandstone under cyclic loading," *Journal of Mountain Science*, vol. 18, no. 12, pp. 3348–3365, 2021.

[5] M. Gao, J. Xie, Y. Gao et al., "Mechanical behavior of coal under different mining rates: A case study from laboratory experiments to field testing," *International Journal of Mining Science and Technology*, vol. 31, no. 5, pp. 825–841, 2021.

[6] D. H. Chen, H. E. Chen, W. Zhang, J. Lou, and B. Shan, "An analytical solution of equivalent elastic modulus considering confining stress and its variables sensitivity analysis for fractured rock masses," *Journal of Rock Mechanics and Geotechnical Engineering*, pp. 1674–7755, 2021.

[7] A. Leemann and R. Loser, "Analysis of concrete in a vertical ventilation shaft exposed to sulfate-containing groundwater for 45years," *Cement and Concrete Composites*, vol. 33, no. 1, pp. 74–83, 2011.

[8] E. Gruyaert, P. Van den Heede, M. Maes, and N. De Belie, "Investigation of the influence of blast-furnace slag on the resistance of concrete against organic acid or sulphate attack by means of accelerated degradation tests," *Cement and Concrete Research*, vol. 42, no. 1, pp. 173–185, 2012.

[9] Y.-c. Zhou, J.-h. Liu, S. Huang, H.-t. Yang, and H.-g. Ji, "Performance change of shaft lining concrete under simulated coastal ultra-deep mine environments," *Construction and Building Materials*, vol. 230, Article ID 116909, 2020.

[10] M. L. Nehdi, A. R. Suleiman, and A. M. Soliman, "Investigation of concrete exposed to dual sulfate attack," *Cement and Concrete Research*, vol. 64, pp. 42–53, 2014.

[11] M. F. Najjar, M. L. Nehdi, A. M. Soliman, and T. M. Azabi, "Damage mechanisms of two-stage concrete exposed to chemical and physical sulfate attack," *Construction and Building Materials*, vol. 137, pp. 141–152, 2017.

[12] Z. Zhang, X. Jin, and W. Luo, "Long-term behaviors of concrete under low-concentration sulfate attack subjected to natural variation of environmental climate conditions," *Cement and Concrete Research*, vol. 116, pp. 217–230, 2019.

[13] T. Aye and C. T. Oguchi, "Resistance of plain and blended cement mortars exposed to severe sulfate attacks," *Construction and Building Materials*, vol. 25, no. 6, pp. 2988–2996, 2011.

[14] C. Zhu, Z. Yan, Y. Lin, F. Xiong, and Z. Tao, "Design and application of a monitoring system for a deep railway foundation pit project," *IEEE Access*, vol. 7, pp. 107591–107601, 2019.

[15] Z. Dou, Y. Liu, X. Zhang et al., "Influence of layer transition zone on rainfall-induced instability of multilayered slope," *Lithosphere*, vol. 2021, no. 4, Article ID 2277284, 2021.

[16] C. Cao, W. Zhang, J. Chen, B. Shan, S. Song, and J. Zhan, "Quantitative estimation of debris flow source materials by integrating multi-source data: A case study," *Engineering Geology*, vol. 291, Article ID 106222, 2021.

[17] Z. Dou, S. Tang, X. Zhang et al., "Influence of shear displacement on fluid flow and solute transport in a 3D rough fracture," *Lithosphere*, vol. 2021, no. 4, Article ID 1569736, 2021.

[18] X. M. Zhou, G. Q. Zhou, Q. S. Hu, and C. Ma, "Model test research on shaft lining built in high pressure rock aquifer," *Chinese Journal of Rock Mechanics and Engineering*, vol. 30, no. 12, pp. 2514–2522, 2011.

[19] Z. S. Yao, G. H. Yu, H. Cheng, and C. X. Rong, "Research on vertical bearing capacity of shaft lining structure of high strength concrete and double steel cylinders in super-thick alluvium," *Rock and Soil Mechanics*, vol. 31, no. 6, pp. 1687–1691, 2010.

[20] Z. S. Yao, H. Cheng, and C. X. Rong, "Experimental study on shift-boring lining of high performance concrete and double steel cylinder in super-deep alluvium," *Chinese Journal of Rock Mechanics and Engineering*, vol. 26, no. S2, pp. 4264–4269, 2007.

[21] Z. S. Yao, H. Chen, and X. B. Ju, "Research and application of high strength steel fiber concrete compound shaft lining with

inner steel plate in deep alluvium shaft repair," *Journal of China Coal Society*, vol. 42, no. 9, pp. 2295–2301, 2017.

[22] C. X. Rong, X. X. Wang, and H. Cheng, "Research on mechanical characteristics of high-strength reinforced concrete shaft lining in deep alluvium," *Chinese Journal of Rock Mechanics and Engineering*, vol. 27, no. S1, pp. 2841–2847, 2008.

[23] Z. S. Yao, "An experimental study on steel fiber reinforced high strength concrete shaft lining in deep alluvium," *Chinese Journal of Rock Mechanics and Engineering*, vol. 24, no. 7, pp. 1253–1258, 2005.

[24] T. Han, W. H. Yang, and Y. L. Ren, "Horizontal ultimate bearing capacity of encased steel concrete shaft lining," *Journal of Mining and Safety Engineering*, vol. 28, no. 2, pp. 181–186, 2011.

[25] B. D. Ding, Z. Y. Han, G. C. Zhang, X. Beng, and Y. Yang, "Flexural toppling mechanism and stability analysis of an anti-dip rock slope," *Rock Mechanics and Rock Engineering*, vol. 54, no. 1, pp. 1–15, 2021.

[26] G. S. Zhao, M. H. Ren, X. H. Qiu, and Q. Xue, "The unified strength theory for plastic limit load analysis of vertical shaft lining," *Advances in Civil Engineering*, vol. 2018, Article ID 1949324, 8 pages, 2018.

[27] X. Z. Lyu and W. M. Wang, "Deformation monitoring and stability analysis of shaft lining in weakly cemented stratum," *Advances in Civil Engineering*, vol. 2018, Article ID 8462746, 18 pages, 2018.

[28] G. Li, Y. Hu, S.-m. Tian, M. weibin, and H.-l. Huang, "Analysis of deformation control mechanism of prestressed anchor on jointed soft rock in large cross-section tunnel," *Bulletin of Engineering Geology and the Environment*, vol. 80, no. 12, pp. 9089–9103, 2021.

[29] J. H. Liu, R. D. Wu, and Y. C. Zhou, "Experiment of bursting liability of deep underground concrete under complex stress conditions," *Journal of China Coal Society*, vol. 43, no. 1, pp. 79–86, 2018.

[30] M. Z. Gao, H. C. Hao, S. N. Xue, L. Tong, and C. Pengfei, "Discing behavior and mechanism of cores extracted from Songke-2 well at depths below 4,500 m," *International Journal of Rock Mechanics and Mining Sciences*, vol. 149, Article ID 104976, 2022.

[31] H. Peng, X. M. Ma, J. J. Jiang, and L. Peng, "Research on stress field and hydraulic fracturing in-situ stress measurement of 1 000 M deep hole in Zhao-Lou coal mine," *Chinese Journal of Rock Mechanics and Engineering*, vol. 30, no. 8, pp. 1638–1645, 2011.

[32] Y. C. Zhou, J. H. Liu, and H. G. Ji, "Study on bursting liability of fiber reinforced shaft lining concrete based on temperature and compound salt," *Materials Reports*, vol. 33, no. 16, pp. 2671–2676, 2019.

[33] H. G. Ji, D. L. Quan, and X. B. Su, "Influence of grouting on stability of supporting structure in deep roadway intersection area," *Journal of Mining and Safety Engineering*, vol. 38, no. 5, pp. 929–936, 2021.

[34] X. F. Yu, Y. R. Zheng, and H. H. Liu, *Stability Analysis of Surrounding Rock Of Underground Engineering*, coal Industry Press, Beijing, China, 1980.

[35] M. W. Lu and X. F. Luo, *The theoretical Basis Of Elasticity*, Tsinghua University Press, Beijing, China, 2001.

[36] Y. F. Wang and Y. P. Liang, "Study on modulus of elasticity and Poisson ratio of high performance concrete," *Journal of Beijing Jiao Tong University*, vol. 28, no. 1, pp. 5–7, 2004.

[37] Y. S. Liu, X. J. Wang, and T. Jin, "Study on the mechanical properties and constitutive relation of steel fiber reinforced concrete," *Journal of University of Science and Technology of China*, vol. 37, no. 7, pp. 717–723, 2007.

[38] H. X. Du and Y. N. Fan, "Meso-structure damage of C60 high performance concrete at high temperature on X-CT," *Journal of Building Materials*, vol. 23, no. 1, pp. 210–215, 2020.